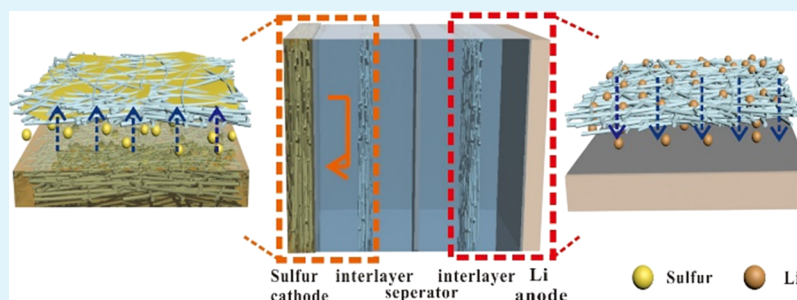


Refining Interfaces between Electrolyte and Both Electrodes with Carbon Nanotube Paper for High-Loading Lithium–Sulfur Batteries

Yueying Peng, Zhipeng Wen, Chaoyue Liu, Jing Zeng, Yunhui Wang, and Jinbao Zhao*[✉]

State-Province Joint Engineering Laboratory of Power Source Technology for New Energy Vehicle, Engineering Research Center of Electrochemical Technology, Ministry of Education, College of Chemistry and Chemical Engineering, Xiamen University, Xiamen 361005, P.R. China

Supporting Information



ABSTRACT: Lithium sulfur (Li–S) batteries are appealing energy storage technologies because of their high theoretical energy density and low cost. However, Li–S batteries suffer from poor practical energy density due to serious polysulfide dissolution and shuttle, as well as lithium anode corrosion. Herein, we provide a dual-protection strategy for the high-energy-density Li–S cell by inserting two nanotube paper (CNTp) interlayers on both electrodes. The CNTp interlayers can provide stable interfaces for both the cathode and anode, facilitating the formation of uniform charge transfer and ion flow. As a result, the Li–S cell exhibits stable cycling performance and great rate ability up to a high rate of 5 C ($5\text{ C} = 25\text{ mA cm}^{-2}$). Even at an ultrahigh sulfur load of 12.1 mg cm^{-2} , a high areal capacity of 12.6 mAh cm^{-2} is still achieved, which can remain at 11.1 mAh cm^{-2} after 30 cycles (corresponding to 917 mAh g^{-1}). The refined interfaces between the electrolyte and both electrodes are further confirmed by the micro-zone current distribution and COMSOL simulation. Our approach provides an effective and universal strategy to improve the electrochemical stability of the Li–S cell at high sulfur load, opening a new platform for designing advanced metal cell systems.

KEYWORDS: lithium–sulfur batteries, high sulfur loads, interlayer, interface, Li anode

1. INTRODUCTION

With the increasing demand for high-energy-density energy storage, much attention has been paid to lithium–sulfur (Li–S) batteries.^{1,2} Li–S batteries, with sulfur as the cathode and Li as the anode, have a high theoretical specific capacity (1675 mAh g^{-1}) and high specific energy density (2600 Wh kg^{-1}).³ Besides, the element sulfur is naturally abundant and environmentally friendly. Therefore, Li–S batteries are considered to be one of the most attractive candidates for the next-generation storage systems.⁴ Nevertheless, the practical commercialization of Li–S cells is still hindered by the low active material utilization, serious electrode structure degradation, fast capacity fading, and safety problems due to the poor electron conductivity of sulfur, polysulfide dissolution and shuttle, large volume expansion during discharging/charging, and Li metal issues.

To overcome the above-mentioned problems, overwhelming efforts have been dedicated on the sulfur cathode because polysulfide dissolution and shuttle are considered to be the most prominent problems.^{5,6} In the process of discharging/

charging, the polysulfides formed in the cathode can easily dissolve into the electrolyte and even react with the Li anode to generate insoluble $\text{Li}_2\text{S}_2/\text{Li}_2\text{S}$ covered on the Li surface, resulting in the loss of active material sulfur and serious corrosion of the Li anode.⁷ Therefore, many studies have been performed to suppress polysulfide dissolution and shuttle, including cathode materials design,^{8,9} separator modification,^{10,11} and electrolyte project.¹² Fabricating sulfur composites can provide great conductive skeleton and strong affinity for sulfur to enhance active material utilization and reduce sulfur loss. However, there are still inevitable polysulfides dissolving in the electrolyte. The separator modification or insertion of interlayers between the cathode and separator functions as the second current collectors to immobilize sulfur and further stop the dissolved polysulfides from approaching the Li anode. The pioneering work is made by Manthiram and

Received: November 12, 2018

Accepted: January 15, 2019

Published: January 15, 2019

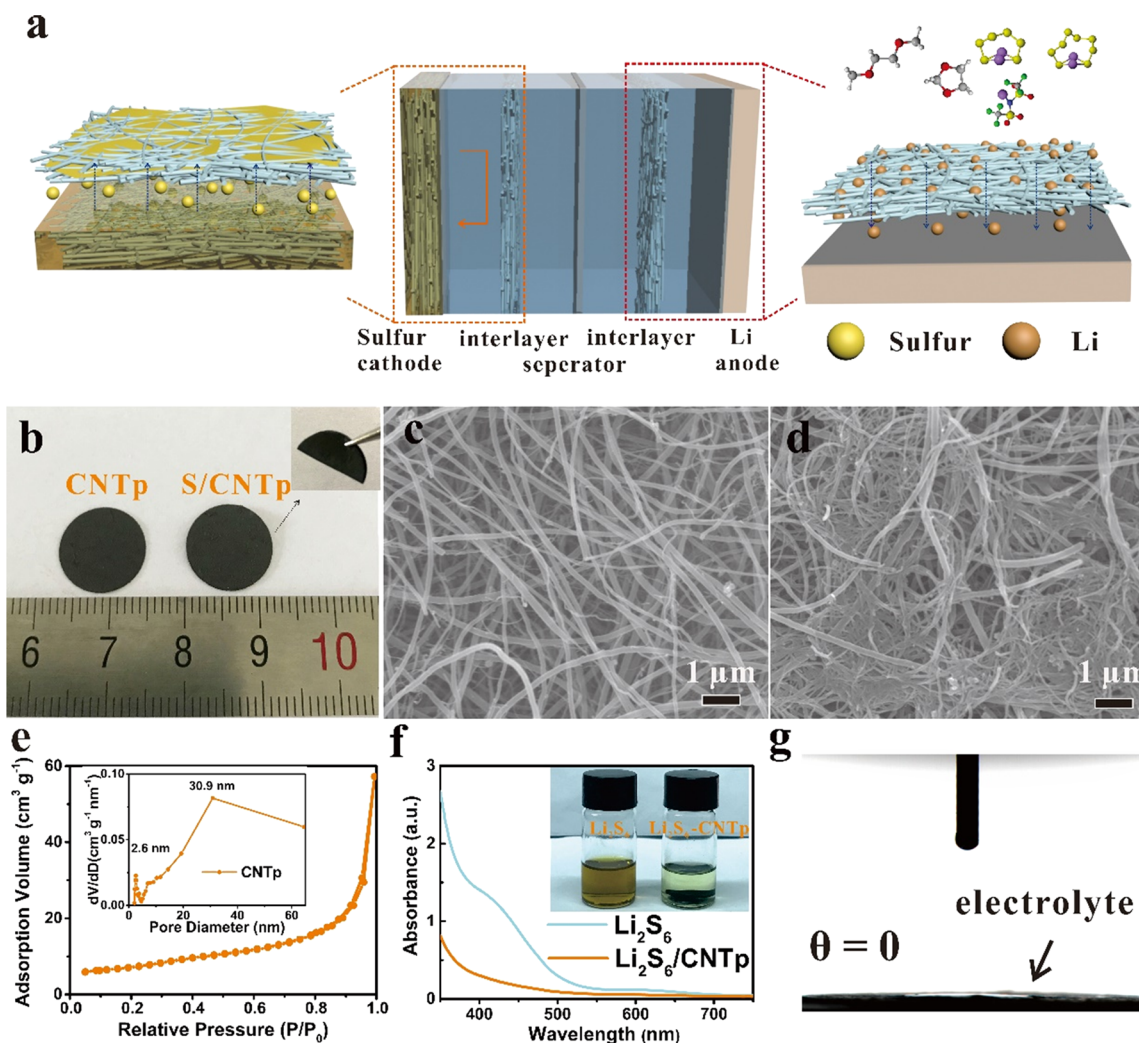


Figure 1. Morphologies and structure characterization. (a) Illustration for the Li–S cell configuration with CNTp interlayers on both electrodes. (b) Optical photographs. (c) SEM image of CNTp. (d) SEM image of the S/CNTp electrode. (e) Nitrogen adsorption/desorption isotherm loop of CNTp (inset: corresponding pore size distribution). (f) UV–Vis absorption spectra (inset: optical photographs of Li_2S_6 solution and Li_2S_6 -CNTp solution). (g) Contact angle of the electrolyte (1 M LiTFSI in DOL/DME) on CNTp.

Su,¹³ who insert a carbon paper between the cathode and separator, achieving enhanced active material utilization and capacity retention. Inspired by this, many other materials, such as carbon materials and organic polymers,^{14–16} have been introduced as interlayers to enhance the electrochemical performances of Li–S cells, demonstrating the efficient strategy of inserting an interlayer to alleviate polysulfide dissolution and shuttle.

Despite the progress of the sulfur cathode, there is still a gap between the practical Li–S cells and the state-of-the-art Li-ion batteries in terms of gravimetric energy density.¹⁷ Increasing sulfur load is one of the primary criteria for high-energy-density Li–S batteries.^{17,18} Thus, numerous strategies have been attempted to design high-sulfur-load electrodes.^{19–21} However, higher sulfur load means that more polysulfides would be generated and more Li sources should be provided, triggering a series of amplification effects.^{22,23} On the one hand, polysulfide dissolution and shuttle will become more serious, leading to low capacity and fast capacity decay. Thus, low active material utilization is normally found, even though high area capacity is obtained.¹⁹ On the other hand, the vast polysulfide dissolution and shuttle will accelerate the unstable

interface between the Li anode and electrolyte, leading to its fast failure.^{24,25} Because of its highly reactive nature, Li can spontaneously react with the electrolyte to generate the solid electrolyte interface (SEI) on the Li anode. The SEI can play as a protected film to prevent the further consumption of Li. Unfortunately, the SEI layer is not strong enough to accommodate volume expansion during the Li stripping/plating process, inducing the nonuniformity of Li stripping/plating, resulting in the formation of Li dendrite.^{26–28} In terms of the Li–S system, the reaction of polysulfides with the Li anode makes this situation more complex.^{24,25,29} As a result, a stable SEI is more difficult to obtain for the Li–S battery. From the above discussion, it can be seen that adopting a high sulfur load is necessary to realize the high-energy-density Li–S cell. However, at high sulfur load, it becomes more challenging to suppress serious polysulfide dissolution and shuttle and obtain a stable Li anode. Therefore, how to effectively protect both the cathode and anode becomes urgently needed for the high-energy-density Li–S cell.

Herein, we develop a dual-protection strategy for both the cathode and anode by inserting two interlayers of nanotube paper (CNTp) in the Li–S battery. First, CNTp, with a special

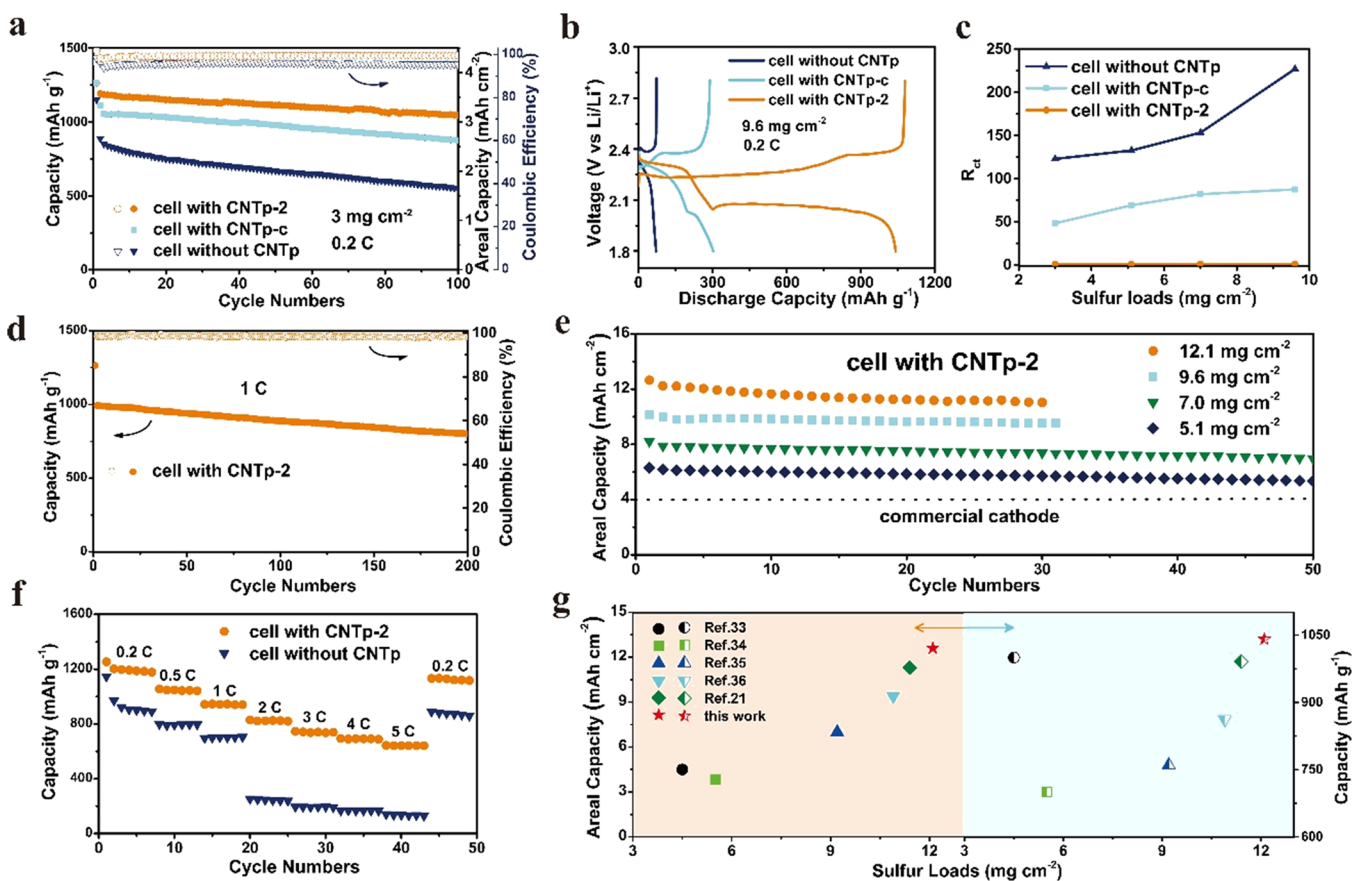


Figure 2. Electrochemical performances. (a) Cycling performances at 0.2 C. (b) Discharge/charge curves at a sulfur load of 9.6 mg cm^{-2} . (c) Comparison of R_{ct} with different sulfur loads. (d) Cycling performance of the cell with CNTp-2 at 1 C. (e) Cycling performances of the cell with CNTp-2 at 0.2 C with high sulfur loads of 5.1, 7.0, 9.6, and 12.1 mg cm^{-2} . (f) Rate performances at different current densities of 0.2, 0.5, 1, 2, 3, 4, and 5 C. (g) Comparison of the initial areal capacity and capacity at 0.2 C with previous reports.^{21,33–36}

mesoporous structure, can provide great affinity for polysulfides. Thus, polysulfide dissolution and shuttle can be effectively suppressed by the two CNTp interlayers. Even if there might be a small amount of polysulfides crossing the separator, the second CNTp inserted between the anode and separator can act as a reinforced barrier to further prevent the polysulfides from reacting with the Li anode. Without polysulfide deterioration, the SEI of the Li anode becomes more stable. Besides, we find that CNTp can refine the interfaces, facilitating the formation of uniform current and Li-ion distribution for the cathode and anode, respectively. As a result, high active material utilization is achieved even at an ultrahigh sulfur load of 12.1 mg cm^{-2} and at a high rate of 5 C (25 mA cm^{-2}). This strategy provides a facile and universal approach to realizing high capacity at high sulfur load, offering a new opportunity to develop the high-energy-density Li–S cell.

2. RESULTS AND DISCUSSION

The cell configuration with two CNTp interlayers on both electrodes is illustrated in Figure 1a. Without the CNTp interlayer, the polysulfides form from the cathode and easily diffuse into the electrolyte, leading to the loss of active materials. What is worse is that these dissolved polysulfides, together with the electrolyte to react with the Li anode, can repeatedly deteriorate the SEI composition of the Li anode, resulting in Li dendrite generation and its final failure. When inserting one CNTp interlayer on the cathode, a majority of

polysulfides will be immobilized in the cathode region. But the Li anode without any protection can still react with the electrolyte to form an unstable SEI. Moreover, to make this situation worse, there might be a few polysulfides crossing the separator, especially at high sulfur load. However, if CNTp is inserted on both the cathode and anode, then the polysulfides can be mainly absorbed by the first CNTp interlayer. Even if there might be a few polysulfides passing through the separator, the second CNTp interlayer can play as a reinforced barrier to further prevent the polysulfides from reacting with the lithium anode. In addition, the three-dimensional (3D) network structure and high electrical conductivity ($4.5 \times 10^4 \text{ S m}^{-1}$) of CNTp can provide a robust electronic and ion transport pathway, aiding the constitution of a stable SEI on the Li anode. Therefore, two CNTp interlayers can not only confine polysulfides but also provide stable interfaces for both the cathode and anode.

Figure 1b–d displays the morphologies of CNTp and S/CNTp. The appearance of CNTp presents a black color. Even after crimping and folding by several times (Figure S1a), CNTp can still well maintain its pristine structure, demonstrating its excellent mechanical strength and flexibility. After infiltrating sulfur into CNTp by the melting method (see details in Materials and Methods), S/CNTp can still maintain great flexibility (inset of Figure 1b). The SEM images in Figure S1b reveal that the pristine CNT has an ultralong length of tens of micrometers, which is the reason for the great flexibility of CNTp and S/CNTp. This is beneficial for the integrity of an

electrode to buffer volume expansion of both the cathode and anode during the discharge/charge process. Further SEM image of CNTp displays its 3D interwoven network structure, which can provide a fast ion transportation pathway. Figure 1d shows that there is obvious sulfur attached to CNTp compared with the smooth surface of pristine CNTp. To demonstrate the adsorption ability of CNTp for polysulfides, nitrogen adsorption/desorption isotherm of CNT is analyzed to get information about its pore structure (Figure 1e). The BET specific surface area is measured to be $25.2 \text{ m}^2 \text{ g}^{-1}$. Further size distribution shows that the pore size is mainly distributed at 2.6 and 30.9 nm. The existence of mesopores in CNTp can provide physical adsorption for polysulfides.^{30,31} Moreover, the summary XPS of pristine CNT reveals the existence of an oxygen (O) atom apart from the carbon (Figure S1c). Previous theoretical calculation has proved that the O-doped carbon matrix can provide stronger adsorption for polysulfides,⁸ suggesting that CNTp can also provide chemical adsorption for polysulfides. In addition, visual experiment is performed to directly observe its adsorption ability. Taking Li_2S_6 as a representative of polysulfides, the color of Li_2S_6 solution changes from brown to almost colorless after adding CNTp (inset of Figure 1f). UV–Vis spectrum in Figure 1f further reveals that there is no Li_2S_6 absorption peak in the upper solution, confirming the great affinity of CNTp to polysulfides. To investigate the hydrophilicity of CNTp for the electrolyte, contact angle test is carried out. As shown in Figure 1g, the contact angle of the electrolyte on CNTp is nearly 0° , suggesting that the electrolyte can perfectly permeate into CNTp. Benefiting from the great hydrophilicity, the amount of electrolyte uptake is measured to be $580 \pm 10\%$. Such large electrolyte uptake can hold large amounts of electrolytes to provide an abundant ion transport pathway when passing through CNTp, facilitating uniform ion flow before reaching the electrode surface.³²

To examine the effects of CNTp on the electrochemical behaviors of Li–S batteries, the cell without a CNTp interlayer (cell without CNTp), the cell with one CNTp interlayer on the cathode (cell with CNTp-c), and the cell with two CNTp interlayers on both the cathode and anode (cell with CNTp-2) are assembled, respectively. Considering that the sulfur load might influence the electrochemical behaviors of the Li–S cell,²² the comparisons are carried out with the same sulfur load. First, the cycling performances for cells at a sulfur load of 3 mg cm^{-2} are compared at 0.2 C ($1 \text{ C} = 1675 \text{ mA g}^{-1}$) (Figure 2a). For the cell without CNTp, fast capacity fading is observed from an initial discharge capacity of $1151.2 \text{ mAh g}^{-1}$ to only 552.8 mAh g^{-1} after 100 cycles. Upon introducing the CNTp interlayer, great improvements of both capacity retention and coulombic efficiency are observed when CNTp is inserted on the cathode side, the anode side (Figure S2), or both sides, indicating the effective adsorption of CNTp for polysulfides to improve sulfur utilization. Among them, the cell with CNTp-2 shows the highest capacity and best cycling stability, with the reversible capacity of $1046.1 \text{ mAh g}^{-1}$ remaining after 100 cycles, demonstrating the efficient role of CNTp on both sides of the anode and cathode. In spite of the high specific capacity, the corresponding areal capacity is recorded to be 3.1 mAh cm^{-2} after 100 cycles with a sulfur load of 3 mg cm^{-2} . To further compete with the practical cathode material of the Li-ion battery (4 mAh cm^{-2}),³⁷ the cells are assembled with higher sulfur loads of 5.1, 7.0, and 9.6 mg cm^{-2} . As shown in Figure S3a,b, with sulfur loads

increasing, large polarization and fast capacity fading are found for the cell without CNTp and the cell with CNTp-c. When the sulfur load is increased to 9.6 mg cm^{-2} , serious polarization (Figure 2b) and fast failure occurred (Figure S3d,e). Such fast fading can be attributed to the intensified shuttle effect of a large amount of polysulfides and the corrosion of the Li anode.²⁹ By contrast, the cell with CNTp-2 shows no obvious polarization even when the sulfur load is increased to 9.6 mg cm^{-2} (Figure 2b). Stable discharge/charge curves can be clearly observed (Figure S3c,f). These results indicate that inserting CNTp on both the cathode and anode can significantly reduce the polarization and enhance the electrochemical stability of the Li–S cell, ensuring that it keeps working even at ultrahigh sulfur load. Because of the poor conductivity of sulfur, high sulfur load might cause the increased interface resistance, resulting in low active material utilization. This hypothesis is supported by the electrochemical impedance spectroscopy (EIS) in Figure S4. The fitting values of charge transfer resistance (R_{ct}) are compared in Figure 2c. With sulfur loading increasing, R_{ct} shows a growing tendency for the cell without CNTp and the cell with CNTp-c. By contrast, the cell with CNTp-2 maintains the stable and small values of R_{ct} . Thus, it is concluded that CNTp can effectively reduce the interface resistance of the Li–S cell, providing a fast and stable charge transfer.

To further demonstrate this conclusion, the cell with CNTp-2 is evaluated at higher current densities. As shown in Figure 2d, a great cycling stability can be still obtained at a high current density of 1 C. After 200 cycles, a discharge capacity of 802.0 mAh g^{-1} still remains with a capacity decay rate of 0.06% per cycle. Further rate ability at different rates of 0.2, 0.5, 1, 2, 3, 4, and 5 C are assessed, respectively (Figure 2f). For the cell without CNTp, fast capacity fading can be found, especially at high rates of 2, 3, 4, and 5 C. Extremely large polarizations are observed from the discharge/charge curves (Figure S5a). By contrast, the cell with CNTp-2 exhibits high discharge capacities of 1202.6, 1056.0, 943.8, 829.1, 745.8, 694.2, and 644.2 mAh g^{-1} at rates of 0.2, 0.5, 1, 2, 3, 4, and 5 C, respectively. Typical discharge/charge curves can be still found even at a high rate of 5 C ($5 \text{ C} = 25 \text{ mA cm}^{-2}$, Figure S5b). When switching the rate back to 0.2 C, a stable capacity of $1132.8 \text{ mAh g}^{-1}$ can be still achieved, indicating the excellent electrode integrity of the cell with CNTp-2. The great rate ability of the cell with CNTp-2 can be attributed to the fast charge transfer in the 3D structure of CNTp, agreeing well with the results from the EIS measurement. The cycling performances of the cell with CNTp-2 at high sulfur loads of 5.1, 7.0, 9.6, and 12.1 mg cm^{-2} are shown in Figure 2e. It can be seen that stable cycling performances are achieved, with high initial areal capacities of 6.3, 8.2, 10.1, and 12.6 mAh cm^{-2} obtained at sulfur loads of 5.1, 7.0, 9.6, and 12.1 mg cm^{-2} , respectively. After 30 cycles, cells with sulfur loads of 9.6 and 12.1 mg cm^{-2} still exhibit high areal capacities of 9.6 and 11.1 mAh cm^{-2} (corresponding to 1000 and 917 mAh g^{-1}), respectively. Compared with previous reports (Figure 2g and Table S1), the cell with CNTp-2 in our work exhibits outstanding electrochemical performances. In spite of seemingly high areal capacities (in mAh cm^{-2}) obtained in a previous work,¹⁹ poor specific capacities (in mAh g^{-1}) are found, reflecting low active material utilization. By contrast, the cell with CNT-2 in our work simultaneously exhibits high and stable areal capacity and specific capacity, suggesting high active material utilization at high sulfur load. Above results

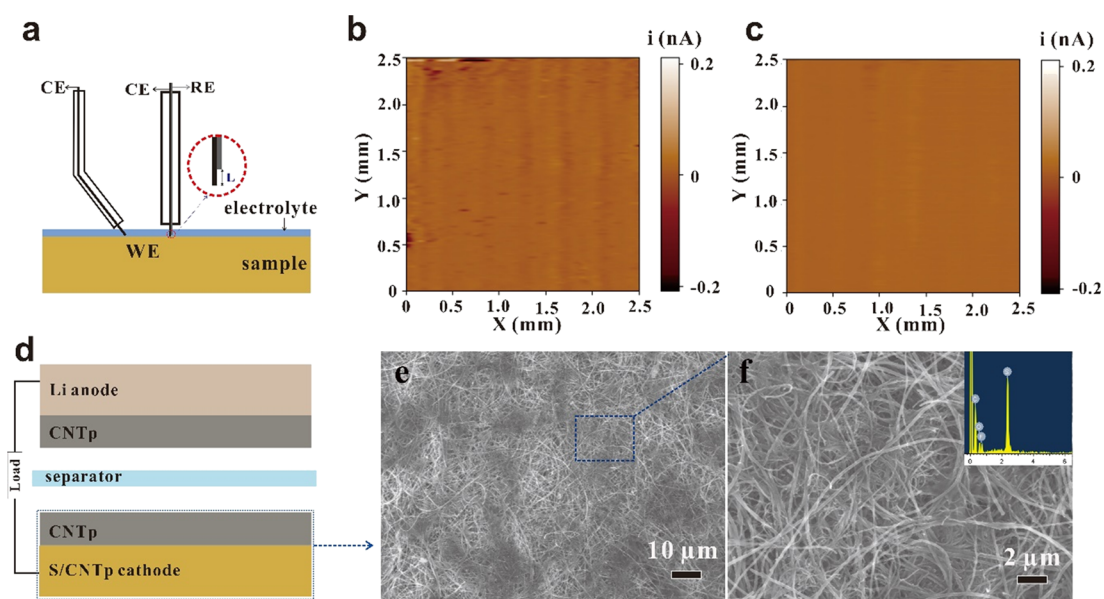


Figure 3. Influence of CNTp on the cathode. (a) Mechanism illustration for the test of micro-zone current distribution using a scanning electrochemical workstation. (b) Micro-zone current distribution for the S/CNTp cathode. (c) Micro-zone current distribution for CNT/S with the CNTp interlayer cathode. (d) Illustration for the tested cathode of the cell with CNTp-2. (e) SEM image of S/CNTp with the CNTp interlayer (the side attached to a separator) at low magnification. (f) SEM images of S/CNTp with the CNTp interlayer cathode at high magnification (inset: EDS image).

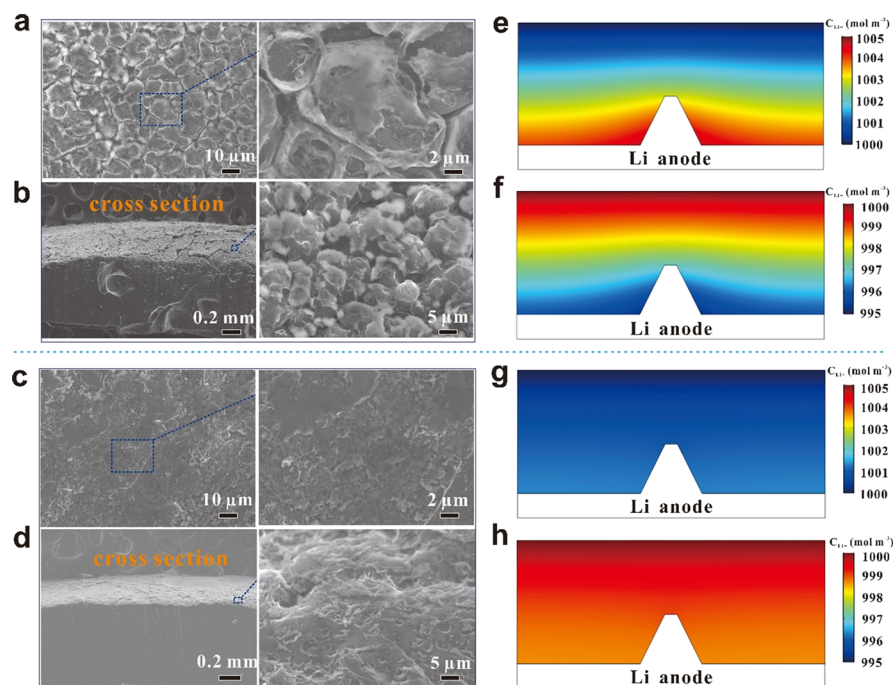


Figure 4. Influence of CNTp on the anode. (a) Top-view SEM images of the Li anode for the cell without CNTp. (b) Cross-section view SEM images of the Li anode for the cell without CNTp. (c) Top-view SEM images of the Li anode for the cell with CNTp-2. (d) Cross-section view SEM images of the Li anode for the cell with CNTp-2. (e, f) Simulation of the Li-ion concentration on the Li anode without a CNTp interlayer: (e) Li stripping and (f) Li plating. (g, h) Simulation of the Li-ion concentration on the Li anode with a CNT interlayer: (g) Li stripping and (h) Li plating.

demonstrate that inserting CNTp on both electrodes can effectively enhance active material utilization, rate performance, and cycling stability at high sulfur load, promising a new strategy for designing the high-energy-density Li–S cell.

To get more information about the great electrochemical performances of the cell with CNTp-2, the impact of CNTp on the sulfur cathode is first investigated. The micro-zone current

distribution on the interface of the cathode/electrolyte is detected using a scanning electrochemical workstation. As illustrated in Figure 3a, the current distribution can be obtained on the basis of dual-probe scanning, which is closely approaching the surface of the sample. More detailed illustration can be found in Supporting Information (Figure S6). The micro-zone current distributions are compared in a

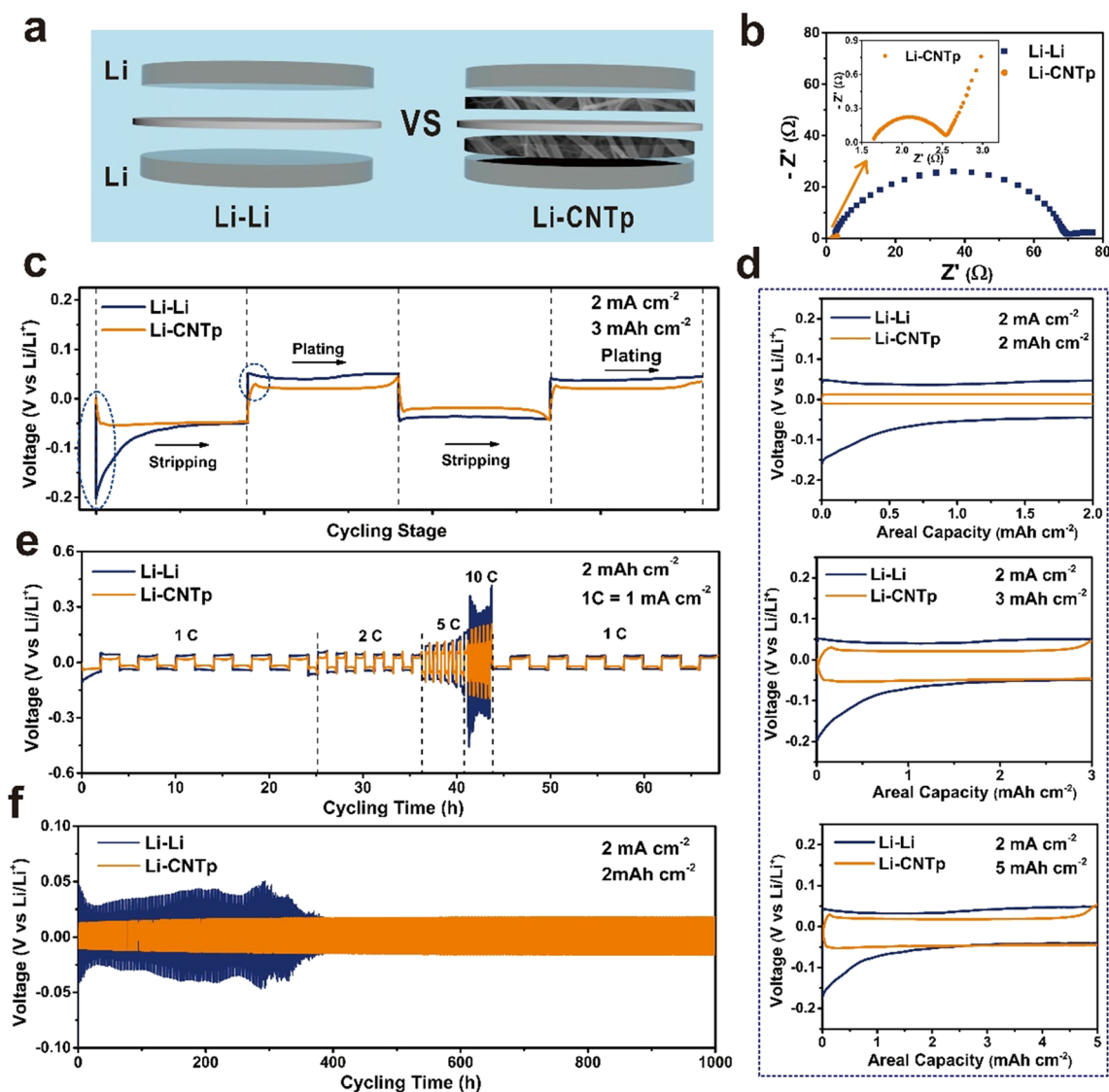


Figure 5. Electrochemical performances of a Li–Li symmetrical cell. (a) Illustration for the assembled Li symmetrical cell. (b) EIS plots. (c) Voltage–time curves at 2 mA cm^{-2} for 3 mAh cm^{-2} . (d) Voltage–capacity curves at 2 mA cm^{-2} with different areal capacities of 2, 3, and 5 mAh cm^{-2} . (e) Rate performances at different current densities of 1, 2, 5, and 10 C. (f) Long cycling performance at 2 mA cm^{-1} for 2 mAh cm^{-2} .

region of $2.5 \text{ mm} \times 2.5 \text{ mm}$ (Figure 3b,c). For the S/CNTp cathode, there are obvious dark color distributions in some discrete areas, reflecting lower current regions. Such nonuniform current distribution suggests the nonuniform utilization of the active material sulfur because of its poor electron conductivity. By contrast, the S/CNTp cathode with the CNTp interlayer shows a uniform current distribution in the whole region. In addition, the function of CNTp on adsorbing polysulfides can be also seen from the SEM images in Figure 3e,f. This reveals that the introduction of CNTp can greatly refine the interface between the cathode and electrolyte, increasing active material utilization.

Furthermore, the morphologies of the Li anode are analyzed to investigate the influence of CNTp on the Li anode. As shown in Figure 4a, the top view of the Li anode for the cell without CNTp exhibits an uneven surface with typical mossy Li after initial cycle, owing to the complex reaction of Li metal with the electrolyte and dissolved polysulfides.³⁸ From the cross-section view (Figure 4b), it can be seen that the wholly utilized Li presents a loose and porous structure, resulting in

the increased surface area of Li, leading to the accelerated reaction of the Li anode with the electrolyte. By contrast, the surface of the Li anode for the cell with CNTp-2 exhibits a smooth and even morphology (Figure 4c). Moreover, an intact and dense morphology is found for the inner used Li (Figure 4d), indicating that uniform Li stripping/plating happens with the aid of CNTp. Even after 100 cycles (Figure S7a,b), the Li anode of the cell with CNTp-2 still maintains a smooth and stable surface, whereas the cell without CNTp presents a seriously rough surface (Figure S7c,d), owing to the repeated reaction of Li with the electrolyte and polysulfides. This demonstrates that a stable SEI of the Li anode can be formed after inserting CNTp. To get the deep understanding about such phenomenon, the distribution of Li-ion concentration is analyzed using the COMSOL simulation. For the bare Li anode, the nonuniform distribution of Li-ion flue can be clearly seen between the Li anode and separator (Figure 4e,f), which results in nonuniform Li stripping/plating and even Li dendrite growth.²⁸ By contrast, after inserting CNTp between the Li anode and separator, uniform distribution of Li ion can be

obtained (Figure 4g,h). This might be benefited from the enlarged surface area and 3D structure of CNTp, which helps lower local current density³⁹ and controls the spatial distribution of Li ion, respectively.⁴⁰ Figure S8 shows a more detailed change process for the Li-ion concentration as time goes on. Taking the Li stripping process as an example, the Li-ion concentration on the Li anode surface gradually increases, whereas after inserting the CNTp interlayer, the Li-ion concentration in the whole stripping process maintains a relatively uniform distribution. The results of simulation give good explanation for the even surface of the Li anode for the cell with CNTp-2, confirming that CNTp can spatially control the distribution of Li ion, refining the interface between the Li anode and electrolyte.

To further demonstrate the effect of CNTp on the interface stability of the Li anode, Li–Li symmetrical cells are assembled (Figure 5a). The EIS plots in Figure 5b show that there is a remarkable decrease in the semicircle after inserting CNTp, implying significantly reduced resistance of the Li/electrolyte interface. The typical voltage profiles of Li stripping/plating are exhibited in Figure 5c. With an areal capacity of 3 mAh cm⁻² at 2 mA cm⁻², the bare Li–Li cell shows a larger overpotential (−0.20 V) than that of Li–CNTp (−0.0058 V) at the initial stripping process, demonstrating the stable interface for Li–CNTp. To further confirm this, the voltage curves of Li stripping/plating are measured with different areal capacities of 2, 3, and 5 mAh cm⁻², respectively (Figure 5d). Notably, the Li–CNTp cell still exhibits slower and more stable voltage plateau than the Li–Li cell in all cases. In addition, Figure 5e compares the voltage plots of the Li-plated/strapped process at different current densities of 1, 2, 5, and 10 mA cm⁻² with the fixed capacity of 2 mAh cm⁻². The Li–CNTp cell still maintains slower voltage hysteresis. Even at a high current density of 10 mA cm⁻², a stable potential plot with a range of −0.1 to 0.09 V is still achieved by Li–CNTp, whereas significant dips and dumps are found in the Li–Li cell. Furthermore, the cycling stability of both Li–Li and Li–CNTp cells is compared in Figure 5f. The Li–Li cell shows a fluctuant potential oscillation with a sudden voltage drop after 400 h cycling. This can be interpreted as the repetitive formation and breakage of the SEI on the Li anode with a short circuit due to Li dendrite formation.⁴¹ By contrast, a much more stable voltage plateau is observed in the Li–CNTp cell. Even after long cycling for 1000 h, there is no observation for the Li dendrite-induced failure, suggesting a stable Li/electrolyte interface. All above results further confirm the conclusion that putting CNTp between the Li anode and separator can greatly refine the interface between the Li anode and electrolyte, providing stable Li stripping/plating.

3. CONCLUSIONS

In summary, the refined interfaces between the electrolyte and both electrodes are formed by inserting two CNTp interlayers for the high-energy-density Li–S cell. Owing to the stable interfaces for effective confinement of the polysulfides on the cathode and facilitation of uniform Li-ion flux on the anode, the Li–S battery, even with an ultrahigh sulfur load of 12.1 mg cm⁻², can still exhibit a high areal capacity of 12.6 mAh cm⁻² at 0.2 C, which still maintains a reversible capacity of 11.1 mAh cm⁻² after 30 cycles. CNTp exhibits a strong ability to adsorb the polysulfides. In addition, micro-zone current measurements reveal that uniform current distribution is formed at the surface of the sulfur cathode after inserting CNTp, enhancing active

material utilization. Furthermore, the smooth and stable Li anode surface is observed with the aid of CNTp to produce uniform Li-ion flux, which is confirmed by the COMSOL simulation. Our strategy suggests that the stable interfaces for both the cathode and anode are vitally important for high sulfur load. We believe that further improvements can be realized by optimizing materials, and such novel cell configuration can be also extended to the other systems, providing a new perspective to design advanced battery systems.

4. MATERIAL AND METHODS

4.1. Synthesis of CNTp and S/CNTp. The CNT powder (0.1 g) was completely dispersed into 400 mL deionized water with 0.2% surfactant Triton X-100 using ultrasonication for 1 h. Then, the required liquid was taken for filtration using a vacuum filter and washed with the deionized water for several times until the surfactant is clear. After drying at 60 °C in a vacuum oven overnight, the freestanding CNT paper (CNTp) can be obtained. The mass of CNTp for the cathode and interlayer is controlled at 3.0 and 1.0 mg cm⁻², respectively. The corresponding thickness of CNTp is measured by digital Vernier (Mitutoyo) to be ~0.100 and ~0.033 mm, respectively.

On the basis of the mass of as-prepared CNT paper, a certain amount of sulfur powder was dissolved into carbon disulfide (CS₂) solution, followed by dropwise addition into CNTp. Finally, S/CNTp was obtained via heating at 155 °C for 3 h under the argon atmosphere. The sulfur load was controlled at 3.0, 5.1, 7.0, 9.6, and 12.1 mg cm⁻², respectively, the thickness of which is measured to be ~0.105, ~0.111, ~0.131, ~0.156, and ~0.210 mm, respectively.

4.2. Synthesis of Li₂S₆ Solution. Li₂S and S powders were added into the mixture solution (1,2-dimethoxyethane (DME) and 1,3-dioxolane (DOL), v/v = 1:1) based on the stoichiometric ratio. After heating at 80 °C for 12 h, a russet solution of Li₂S₆ can be obtained. All above operations were conducted in an argon-filled glove box.

4.3. Characterization. The SEM images were characterized using HITACHI S-4800. Nitrogen isothermal adsorption/desorption plot was obtained by Micromeritics 2020 to give the information about Brunauer–Emmett–eller (BET) specific surface area and pore structure. The ultraviolet–visible (UV-Vis) spectra were carried out on a UV–Vis spectrophotometer (UV 2450). A scanning electrochemical workstation (Xiamen Legang Materials Technology Company) was used to detect the micro-zone current distribution on the surface of the cathode.

4.4. Cell Assembly and Electrochemical Measurement. S/CNTp was cut into disks with 12 mm diameter and used as the cathode. Li metal was used as both the reference and counter electrodes. The electrolyte was the mixture of 1.0 M bis-(trifluoromethanesulfonyl)imide lithium (LiTFSI) in DME and DOL (1:1, v/v) with 1% LiNO₃. The CNTp interlayer was cut into 16 mm disks. The CR2032 coin cell was assembled in an argon-filled glove box. The ratio of the electrolyte to sulfur is controlled at 15:1 μL mg⁻¹. The cell without the CNTp interlayer, the cell with one CNTp between the cathode and separator, the cell with one CNTp between the anode and separator, and the cell with two CNTp interlayers on both sides are named as the cell without CNTp, the cell with CNTp-c, the cell with CNTp-a, and the cell with CNTp-2, respectively. The total mass of the CNTp interlayer for the cell with CNTp-2 was controlled as the same as the cell with CNTp-c (2 mg cm⁻²). The discharge and charge process was performed on battery system (LAND CT2001A instrument, China). The Autolab electrochemical workstation was adopted to obtain electrochemical impedance spectra (EIS) with the frequency range of 0.1 Hz to 100 KHz.

4.5. Simulation in COMSOL. The electrochemical models are constructed in COMSOL Multiphysics. Both models consist of two domains. The lower one represents lithium electrode, with a protrusion on the surface representing lithium dendrite. The upper

domain represents the separator and CNTp interlayer. The physics interface used in the model is “Tertiary Current Distribution, Nernst-Planck”. The separator is treated as an inert porous structure filled with electrolytes. The porous character of separator will reduce the effective diffusion coefficient based on eq 1

$$D_{\text{eff}} = D \times \varepsilon^{\text{brugg}} \quad (1)$$

where D is the diffusion coefficient of Li ion, which is $1 \times 10^{-9} \text{ m}^2 \text{ s}^{-1}$. D_{eff} is the effective diffusion coefficient of Li ion. ε is the porosity, which is set to be 0.6. The brugg represents the tortuosity, which is 1.5. The same domain is used in the second model, which is inserted with a CNTp interlayer. The porosity and electronic conductivity of CNTp are considered in the simulation. For the Li anode, Ohm's law is applied. The electronic conductivity of Li is $1 \times 10^7 \text{ S m}^{-1}$. Butler–Volmer equation is applied on the Li surface to describe the lithium deposition and dissolution process. The lithium electrode thickness is set to $2 \mu\text{m}$. The protrusion is $5 \mu\text{m}$ wide and $4 \mu\text{m}$ high.

■ ASSOCIATED CONTENT

● Supporting Information

The Supporting Information is available free of charge on the ACS Publications website at DOI: 10.1021/acsami.8b19866.

SEM and XPS of pristine CNT, cycling performance, initial discharge/charge curves, EIS measurement, illustration for the scanning electrochemical workstation, SEM of the Li anode after 100 cycles, simulation of Li-ion concentration for Li stripping (PDF)

■ AUTHOR INFORMATION

Corresponding Author

*E-mail: jbzhaoy@xmu.edu.cn.

ORCID

Jinbao Zhao: 0000-0002-2753-7508

Notes

The authors declare no competing financial interest.

■ ACKNOWLEDGMENTS

This work is supported by the National Natural Science Foundation of China (grant nos. 2127318 and 21621091) and the National Key Research and Development Program of China (2017YFB0102000). The authors also wish to express their thanks to Prof. Daiwei Liao and Prof. Weidong He for their valuable suggestions.

■ REFERENCES

- (1) Bruce, P. G.; Freunberger, S. A.; Hardwick, L. J.; Tarascon, J. M. Li–O₂ and Li–S Batteries with High Energy Storage. *Nat. Mater.* **2012**, *11*, 19–29.
- (2) Seh, Z. W.; Sun, Y.; Zhang, Q.; Cui, Y. Designing High-Energy Lithium–Sulfur Batteries. *Chem. Soc. Rev.* **2016**, *45*, 5605–5634.
- (3) Manthiram, A.; Chung, S.-H.; Zu, C. Lithium–Sulfur Batteries: Progress and Prospects. *Adv. Mater.* **2015**, *27*, 1980–2006.
- (4) Pang, Q.; Liang, X.; Kwok, C. Y.; Nazar, L. F. Review—The Importance of Chemical Interactions between Sulfur Host Materials and Lithium Polysulfides for Advanced Lithium–Sulfur Batteries. *J. Electrochem. Soc.* **2015**, *162*, A2567–A2576.
- (5) Wild, M.; O'Neill, L.; Zhang, T.; Purkayastha, R.; Minton, G.; Marinescu, M.; Offer, G. J. Lithium Sulfur Batteries, a Mechanistic Review. *Energy Environ. Sci.* **2015**, *8*, 3477–3494.
- (6) Huang, J.-Q.; Zhang, Q.; Wei, F. Multi-Functional Separator/Interlayer System for High-Stable Lithium–Sulfur Batteries: Progress and Prospects. *Energy Storage Mater.* **2015**, *1*, 127–145.
- (7) Mikhaylik, Y. V.; Akridge, J. R. Polysulfide Shuttle Study in the Li/S Battery System. *J. Electrochem. Soc.* **2004**, *151*, A1969–A1976.
- (8) Peng, Y.; Zhang, Y.; Huang, J.; Wang, Y.; Li, H.; Hwang, B. J.; Zhao, J. Nitrogen and Oxygen Dual-Doped Hollow Carbon Nanospheres Derived from Catechol/Polyamine as Sulfur Hosts for Advanced Lithium Sulfur Batteries. *Carbon* **2017**, *124*, 23–33.
- (9) Peng, Y.; Zhang, Y.; Wen, Z.; Wang, Y.; Chen, Z.; Hwang, B.-J.; Zhao, J. Constructing Fast Electron and Ion Conductive Framework for Li₂S as Advanced Lithium Sulfur Battery. *Chem. Eng. J.* **2018**, *346*, 57–64.
- (10) Shao, H.; Wang, W.; Zhang, H.; Wang, A.; Chen, X.; Huang, Y. Nano-TiO₂ Decorated Carbon Coating on the Separator to Physically and Chemically Suppress the Shuttle Effect for Lithium–Sulfur Battery. *J. Power Sources* **2018**, *378*, 537–545.
- (11) Shi, L.; Zeng, F.; Cheng, X.; Lam, K. H.; Wang, W.; Wang, A.; Jin, Z.; Wu, F.; Yang, Y. Enhanced Performance of Lithium–Sulfur Batteries with High Sulfur Loading Utilizing Ion Selective MWCNT/SPANI Modified Separator. *Chem. Eng. J.* **2018**, *334*, 305–312.
- (12) Yang, H.; Naveed, A.; Li, Q.; Guo, C.; Chen, J.; Lei, J.; Yang, J.; Nuli, Y.; Wang, J. Lithium Sulfur Batteries with Compatible Electrolyte both for Stable Cathode and Dendrite-Free Anode. *Energy Storage Mater.* **2018**, *15*, 299–307.
- (13) Su, Y.-S.; Manthiram, A. Lithium–Sulphur Batteries with a Microporous Carbon Paper as a Bifunctional Interlayer. *Nat. Commun.* **2012**, *3*, 1166.
- (14) Peng, Y.; Zhang, Y.; Wang, Y.; Shen, X.; Wang, F.; Li, H.; Hwang, B.-J.; Zhao, J. Directly Coating a Multifunctional Interlayer on the Cathode via Electrospinning for Advanced Lithium–Sulfur Batteries. *ACS Appl. Mater. Interfaces* **2017**, *9*, 29804–29811.
- (15) Liu, Y.; Qin, X.; Zhang, S.; Liang, G.; Kang, F.; Chen, G.; Li, B. Fe₃O₄-Decorated Porous Graphene Interlayer for High-Performance Lithium–Sulfur Batteries. *ACS Appl. Mater. Interfaces* **2018**, *10*, 26264–26273.
- (16) Tan, L.; Li, X.; Wang, Z.; Guo, H.; Wang, J. Lightweight Reduced Graphene Oxide@MoS₂ Interlayer as Polysulfide Barrier for High-Performance Lithium–Sulfur Batteries. *ACS Appl. Mater. Interfaces* **2018**, *10*, 3707–3713.
- (17) Hagen, M.; Hanselmann, D.; Ahlbrecht, K.; Maça, R.; Gerber, D.; Tübke, J. Lithium–Sulfur Cells: The Gap between the State-of-the-Art and the Requirements for High Energy Battery Cells. *Adv. Energy Mater.* **2015**, *5*, 1401986.
- (18) Pope, M. A.; Aksay, I. A. Structural Design of Cathodes for Li-S Batteries. *Adv. Energy Mater.* **2015**, *5*, 1500124.
- (19) Luo, L.; Manthiram, A. Rational Design of High-Loading Sulfur Cathodes with a Poached-Egg-Shaped Architecture for Long-Cycle Lithium–Sulfur Batteries. *ACS Energy Lett.* **2017**, *2*, 2205–2211.
- (20) Chung, S.-H.; Chang, C.-H.; Manthiram, A. A Core–Shell Electrode for Dynamically and Statically Stable Li–S Battery Chemistry. *Energy Environ. Sci.* **2016**, *9*, 3188–3200.
- (21) Qie, L.; Manthiram, A. A Facile Layer-by-Layer Approach for High-Areal-Capacity Sulfur Cathodes. *Adv. Mater.* **2015**, *27*, 1694–1700.
- (22) Brückner, J.; Thieme, S.; Grossmann, H. T.; Dörfner, S.; Althues, H.; Kaskel, S. Lithium–Sulfur Batteries: Influence of C-rate, Amount of Electrolyte and Sulfur Loading on Cycle Performance. *J. Power Sources* **2014**, *268*, 82–87.
- (23) Peng, H.-J.; Huang, J.-Q.; Cheng, X.-B.; Zhang, Q. Review on High-Loading and High-Energy Lithium–Sulfur Batteries. *Adv. Energy Mater.* **2017**, *7*, 1700260.
- (24) Lv, D.; Zheng, J.; Li, Q.; Xie, X.; Ferrara, S.; Nie, Z.; Mehdi, L. B.; Browning, N. D.; Zhang, J.-G.; Graff, G. L.; Liu, J.; Xiao, J. High Energy Density Lithium–Sulfur Batteries: Challenges of Thick Sulfur Cathodes. *Adv. Energy Mater.* **2015**, *5*, 1402290.
- (25) Chen, X.; Hou, T.-Z.; Li, B.; Yan, C.; Zhu, L.; Guan, C.; Cheng, X.-B.; Peng, H.-J.; Huang, J.-Q.; Zhang, Q. Towards Stable Lithium–Sulfur Batteries: Mechanistic Insights into Electrolyte Decomposition on Lithium Metal Anode. *Energy Storage Mater.* **2017**, *8*, 194–201.
- (26) Aurbach, D.; Zinigrad, E.; Cohen, Y.; Teller, H. A Short Review of Failure Mechanisms of Lithium Metal and Lithiated Graphite Anodes in Liquid Electrolyte Solutions. *Solid State Ionics* **2002**, *148*, 405–416.

(27) Cheng, X.-B.; Zhang, R.; Zhao, C.-Z.; Zhang, Q. Toward Safe Lithium Metal Anode in Rechargeable Batteries: A Review. *Chem. Rev.* **2017**, *117*, 10403–10473.

(28) Wei, S.; Choudhury, S.; Tu, Z.; Zhang, K.; Archer, L. A. Electrochemical Interphases for High-Energy Storage Using Reactive Metal Anodes. *Acc. Chem. Res.* **2018**, *51*, 80–88.

(29) Qie, L.; Zu, C.; Manthiram, A. A High Energy Lithium-Sulfur Battery with Ultrahigh-Loading Lithium Polysulfide Cathode and its Failure Mechanism. *Adv. Energy Mater.* **2016**, *6*, 1502459.

(30) Lee, J. S.; Kim, W.; Jang, J.; Manthiram, A. Sulfur-Embedded Activated Multichannel Carbon Nanofiber Composites for Long-Life, High-Rate Lithium–Sulfur Batteries. *Adv. Energy Mater.* **2017**, 1601943.

(31) Tang, J.; Liu, J.; Li, C.; Li, Y.; Tade, M. O.; Dai, S.; Yamauchi, Y. Synthesis of Nitrogen-Doped Mesoporous Carbon Spheres with Extra-Large Pores through Assembly of Diblock Copolymer Micelles. *Angew. Chem., Int. Ed.* **2015**, *54*, 588–593.

(32) Cheng, X.-B.; Hou, T.-Z.; Zhang, R.; Peng, H.-J.; Zhao, C.-Z.; Huang, J.-Q.; Zhang, Q. Dendrite-Free Lithium Deposition Induced by Uniformly Distributed Lithium Ions for Efficient Lithium Metal Batteries. *Adv. Mater.* **2016**, *28*, 2888–2895.

(33) Zhou, W.; Guo, B.; Gao, H.; Goodenough, J. B. Low-Cost Higher Loading of a Sulfur Cathode. *Adv. Energy Mater.* **2016**, *6*, 1502059.

(34) Zu, C.; Manthiram, A. High-Performance Li/Dissolved Polysulfide Batteries with an Advanced Cathode Structure and High Sulfur Content. *Adv. Energy Mater.* **2014**, *4*, 1400897.

(35) Li, G.; Lei, W.; Luo, D.; Deng, Y.; Deng, Z.; Wang, D.; Yu, A.; Chen, Z. Stringed “Tube on Cube” Nanohybrids as Compact Cathode Matrix for High-Loading and Lean-Electrolyte Lithium–Sulfur Batteries. *Energy Environ. Sci.* **2018**, *11*, 2372–2381.

(36) Yuan, Z.; Peng, H.-J.; Huang, J.-Q.; Liu, X.-Y.; Wang, D.-W.; Cheng, X.-B.; Zhang, Q. Hierarchical Free-Standing Carbon-Nanotube Paper Electrodes with Ultrahigh Sulfur-Loading for Lithium-Sulfur Batteries. *Adv. Funct. Mater.* **2014**, *24*, 6105–6112.

(37) Song, J.; Xu, T.; Gordin, M. L.; Zhu, P.; Lv, D.; Jiang, Y.-B.; Chen, Y.; Duan, Y.; Wang, D. Nitrogen-Doped Mesoporous Carbon Promoted Chemical Adsorption of Sulfur and Fabrication of High-Areal-Capacity Sulfur Cathode with Exceptional Cycling Stability for Lithium-Sulfur Batteries. *Adv. Funct. Mater.* **2014**, *24*, 1243–1250.

(38) Li, W.; Yao, H.; Yan, K.; Zheng, G.; Liang, Z.; Chiang, Y.-M.; Cui, Y. The Synergetic Effect of Lithium Polysulfide and Lithium Nitrate to Prevent Lithium Dendrite Growth. *Nat. Commun.* **2015**, *6*, 7436.

(39) Zuo, T. T.; Wu, X. W.; Yang, C.-P.; Yin, Y.-X.; Ye, H.; Li, N.-W.; Guo, Y.-G. Graphitized Carbon Fibers as Multifunctional 3D Current Collectors for High Areal Capacity Li Anodes. *Adv. Mater.* **2017**, *29*, 1700389.

(40) Yang, C.-P.; Yin, Y.-X.; Zhang, S.-F.; Li, N.-W.; Guo, Y.-G. Accommodating Lithium into 3D Current Collectors with a Submicron Skeleton Towards Long-Life Lithium Metal Anodes. *Nat. Commun.* **2015**, *6*, 8058–8067.

(41) Liang, Z.; Lin, D.; Zhao, J.; Lu, Z.; Liu, Y.; Liu, C.; Lu, Y.; Wang, H.; Yan, K.; Tao, X.; Cui, Y. Composite Lithium Metal Anode by Melt Infusion of Lithium into a 3D Conducting Scaffold with Lithiophilic Coating. *Proc. Natl. Acad. Sci.* **2016**, *113*, 2862–2867.